Direct validation of the dune instability theory

C. Narteau *Université Paris Cité, Institut de Physique du Globe de Paris, CNRS, France – narteau@ipgp.fr*
P. Lü *School of Geography and Tourism, Shaanxi Normal University, China – lvping@lzb.ac.cn*
P. Claudin *ESPCI, PSL Univ, Sorbonne Univ, Univ Paris Cité, CNRS, France – claudin@pmmh.espci.fr*
Z. Dong *School of Geography and Tourism, Shaanxi Normal University, China – dongzb@lzb.ac.cn*
S. Rodriguez *Université Paris Cité, Institut de Physique du Globe de Paris, CNRS, France – rodriguez@ipgp.fr*
C. Gadal *Université Paris Cité, Institut de Physique du Globe de Paris, CNRS, France – gadal@ipgp.fr*
S. Courrech du Pont *MSC, Université Paris Cité, CNRS, France – sylvain.courrech@u-paris.fr*

ABSTRACT: We designed a landscape-scale experiment at the edge of the Gobi desert, China, to quantify the development of incipient dunes under the natural action of winds. We identified two successive phases, from the initial flat sand bed to a meter-high periodic pattern. During the initial phase, we measure the growth rate of dunes of different wavelengths. We identify the existence of a maximum growth rate, which readily explains the mechanism by which dunes select their size, leading to the prevalence of a 15 m wavelength pattern. We quantitatively compare our experimental results to the prediction of the dune instability theory using transport and flow parameters independently measured in the field. The remarkable agreement between theory and observations demonstrates that the linear regime of dune growth is permanently expressed on low-amplitude bed topography, before larger regular patterns and slip faces eventually emerge.

1 INTRODUCTION

Dune research has always been stimulated by the question of the origin of periodic bedforms that are ubiquitous in rivers, oceans and planetary sand seas. However, the size-selection mechanism leading to the emergence of periodic dunes have never been observed and quantified in a natural environment .

Underwater experiments have shown that, as soon as the flow is strong enough to transport grains, a flat sand bed destabilizes into periodic bedforms migrating at a constant speed (Kennedy 1963). Wind tunnel experiments and Ralph Bagnold's attempts in the field to create artificial dunes have failed because the initial sand piles were not large enough (Bagnold 1941). There is indeed a minimum length-scale for the formation of dunes, which has been estimated to be of the order of 10 m in aeolian systems on Earth based on the smallest wavelength of the superimposed bedforms observed on the flanks of large dunes (Elbelrhiti 2005). After 20 years of intensive research, this characteristic length-scale is assumed to be regulated by the balance between a destabilizing process associated with the turbulent flow response to the topography and a stabilizing process due to transport inertia.

Linear stability analysis of flat sand beds sheared by a fluid flow provide the so-called dispersion relation (Andreotti et al. 2002, Narteau et al. 2009, Gadal et al. 2019, Charru et al. 2013), i.e., the growth rates $\sigma(k)$ of sinusoidal bed perturbations over the whole range of possible wave numbers k (wavelength $\lambda=2\pi/k$). These stability analysis are by definition restricted to the linear regime of incipient dune growth, the period during which the amplitude of each mode (wavelength) grows exponentially and independently from one another. The theoretical relation writes

$$\sigma(k)=Qk^2(B-Akl_{\mathrm{sat}})/(1+(kl_{\mathrm{sat}})^2) \qquad (1)$$

where Q is the mean sand flux and l_{sat} the distance downwind required for the sand flux to reach saturation (i.e., transport inertia). The perturbation of wind streamlines near the bed, in the so-called inner layer, is described with the aerodynamic parameters A and B, so that the upwind shift between the wind speed and the bed topography can be expressed as $\arctan(B/A)/k$.

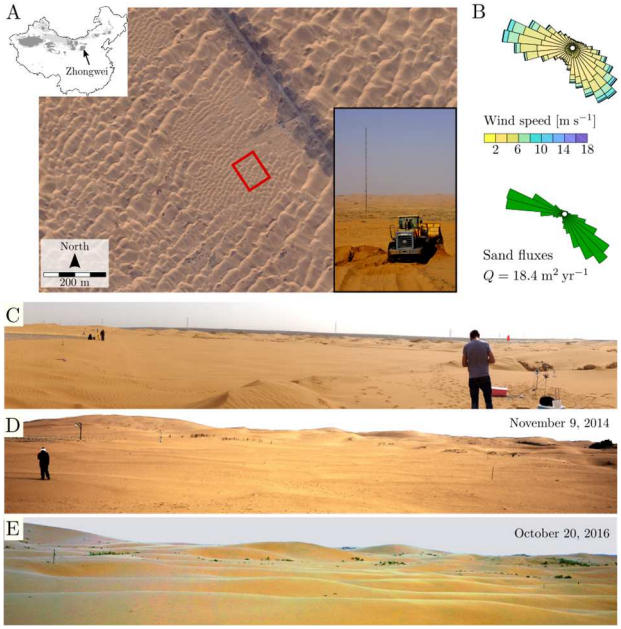

Figure 1. (A) The landscape-scale experiment site in the Tengger desert (37°33’38’’N, 105°2’0.8’’E). The red square shows the location of the flat sand bed experiment. (B) Wind and sand flux roses. (C) The sand bed after flattening. (D) Incipient dunes at the end of the linear phase of dune growth. (E) Mature dunes during the non-linear phase.

Here we present the results of a long-term field experiment in which we have been able to measure in the same desertic area all these parameters. Thus, we obtain a comprehensive description of incipient dune growth under the natural action of wind, which is directly confronted to the dune instability theory (Lü et al. 2021).

2 A LANDSCAPE-SCALE EXPERIMENT

Landscape-scale experiments started in 2009 in the Tengger desert at the southeastern edge of the Gobi basin in China (Fig. 1A, Ping et al. 2014). The experiment dedicated to incipient dune growth has been conducted from April 2014 to November 2017. Preexisting dunes were leveled on 9 April 2014 to form a flat rectangular bed 100 m long and 75 m wide (Fig. 1C). We monitored dune growth over the following 42 mo (Fig. 1D,E) through a series of 20 topographic surveys using a ground-based laser scanner (Lü et al. 2021; Lü et al. 2022). To get a better resolution on the early stage of dune growth and to account for windy periods, these topographic data are not regularly distributed in time and are more frequent in 2014 as well as in the spring and fall of each year. To compare datasets from different scans, we installed a reference system of concrete posts over the entire experimental dune field.

3 RESULTS

3.1 Sand transport properties

As in most of the Tengger desert, the mean grain size in the experimental area is of about 190 μm. Using an impact sensor placed above a flat sand bed, we monitored saltation activity under winds of varying strength. As shown in Fig. 2, the empirical relation between wind speed and the impact rate yields an estimated threshold wind speed for aerodynamic entrainment of sand grains, u_{th}=0.23±0.04 m s^{-1}. Combining this threshold value with local wind data, we calculate the saturated sand flux on a flat sand bed using the eolian transport law of Ungar and Haff (1987). From January 2014 to November 2017, the mean flux is Q=18.4±4.2 m^2 y^{-1}.

To estimate the saturation length, l_{sat}, we constructed a flat bed armored with coarse gravels and cobbles, which acted as a sand trap. At a time without active transport, we build a 12-m-long, 3-m-wide, and 20-cm-high flat sand berm immediately downwind of the coarse bed, as determined from the direction of the prevailing wind. We measure the surface elevation of this sand berm using the terrestrial laser scanner before and after a wind event. The difference in topography along the wind direction gives the mean transport rate profile for this time interval. There is a net erosion on the whole sand slab, with an amplitude that dampens with respect to the downwind distance from the nonerodible bed. These observations indicate an increasing sand flux converging toward its saturated value. Assuming an exponential relaxation of the sand flux (Andreotti et al., 2010), we obtain l_{sat}=0.95±0.2 m (Lü et al. 2021).

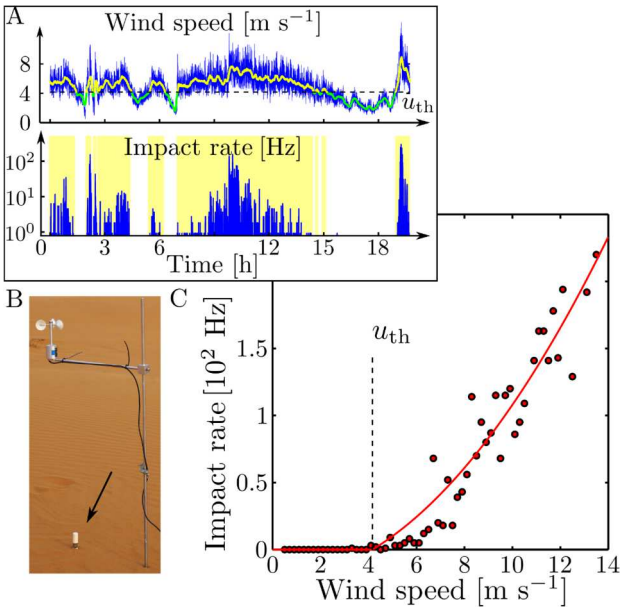

Figure 2. (A) Grain impact rate and wind speed with respect to time. (B) Picture of the impact sensor placed above a flat sand and below a cup anemometer. (C) Relationship between grain impact rate and wind speed u. The solid line is the best fit of $(u^2-u_{th}^2)$ to the data with a critical entrainment threshold u_{th}=4.16 m s^{-1}. Periods above the transport threshold are highlighted in yellow in (A).

3.2 The upwind shift in wind speed

To estimate the values of the aerodynamic parameters A and B used in Eq. 1, we measured the flow properties on dunes of small amplitude. We recorded wind speed at heights of 4, 12, 50, and 100 cm above the bed by moving an anemometer mast upwind of a known elevation dune profile (Fig. 3A). The wind speeds measured at different heights were synchronized and normalized by the wind speed measured at 1 m high by a reference cup anemometer located at the top of a larger dune in the vicinity, which allowed us to reconstruct the perturbation in wind speed on low dunes at different stages of dune growth. As predicted in the limit of low sinusoidal bedforms, Fig. 3B shows that the wind perturbation at all heights reflects the topography of the underlying incipient dunes, both in amplitude and wavelength. The amplitude of perturbation in wind speed decreases with height above the bed. More importantly, there is always an upwind shift in wind speed for the two bottom anemometers at heights of 4 and 12 cm but not for the two top anemometers at heights of 50 and 100 cm. This indicates that, on incipient dunes in our experimental area, the thickness l of the inner layer is between 12 and 50 cm. Within this inner layer, using the upwind shift (≈1 m) and the amplitude of the perturbation in wind speed recorded by the two bottom anemometers, we get A=3±1 and B=1.5±0.5 for dune aspect ratios varying from 0.012 to 0.025 (Fig 3C).

3.3 Emergence of a periodic dune pattern

Within the experimental plot, we select a central rectangular area with a width of 48 m and a length of 82 m (red square in Fig. 1A). The long side of this rectangle is oriented northwest–southeast to align with the prevailing transport direction. We remove the mean slope of this rectangular area by fitting a plane to the elevation data. Throughout the experiment, this plane maintained a gentle southwest-facing slope as observed after the flattening of the dune field. The residual topography is shown for different times in Fig. 4. Within the observation area, we chose to follow the time evolution of elevation along 34 parallel transects with a constant spacing of 1.4 m. These transects are oriented perpendicularly to the final dune orientation observed in November 2017. Fig. 4 shows the elevation profiles with respect to time for a given transect. Over the 42 mo of the experiment, the amplitude of the dunes increases by two orders of magnitude from a few centimeters to a few meters. Whereas no periodic pattern is discernible after flattening, a characteristic wavelength of 15 m emerges over the first few months of the experiment (Fig. 1D,E). The variation of the mean amplitude of the dune pattern, defined as the rms of the topography, is not homogeneous over time and displays a sudden change in rate at the end of 2014 (Fig. 4). Before, from April to October 2014, this amplitude stays almost constant. During this time period, despite a smoother topography, there is nothing to suggest that dunes will appear at a specific wavelength. Starting in November 2014, the surface elevation exhibits a periodic dune pattern with marked crestlines and a northeast-southwest orientation.

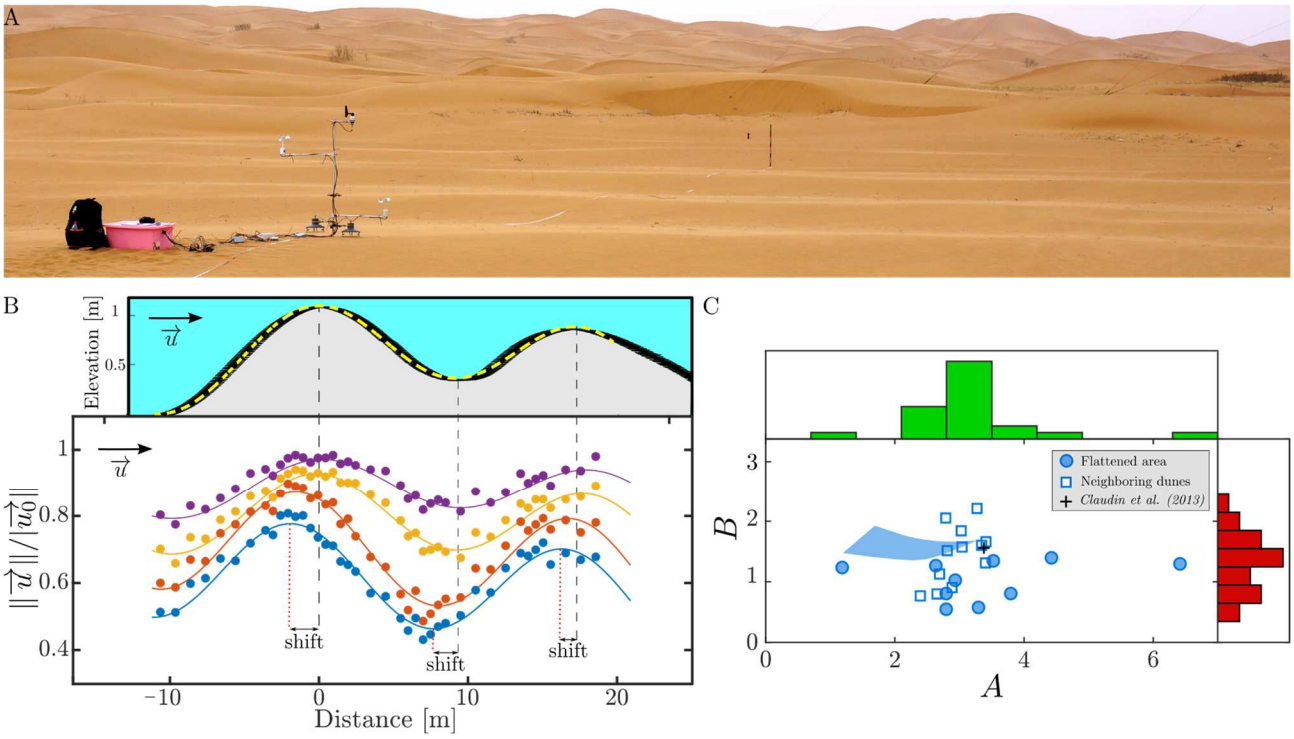

Figure 4. The upwind velocity shift on low sinusoidal bedforms. (A) The mobile anemometer mast, with anemometers located at heights of 4 and 12 cm inthe inner layer and at heights of 50 and 100 cm in the outer layer. The decameter aligned with the mean wind direction gives the direction followed during the successive measurements on sinusoidal incipient dunes. (B) Elevation and normalized wind speed according to distance along the dune profile (blue, red, yellow, and purple for anemometers at 4, 12, 50, and 100 cm, respectively). The normalized wind speed is the wind speed measured along the profile divided by the one recorded by the reference anemometer. Note the upwind shift in wind speed in the inner layer near the bed but not in the outer layer above. Dashed lines show the two dune crests and the trough along the elevation profile. Dotted lines show the maximum and minimum wind speeds in the inner layer. (C) Aerodynamic parameters *A* and *B* measured during dune growth (circles) and on neighboring dunes (squares). The blue area shows the best-fit values of *A* and *B* to the experimental dispersion relation shown in Fig. 5B for $0.6< l_{sat}<1.2$. The distributions of *A* and *B* are illustrated by green and red histograms, respectively.

Then, the mean amplitude increases significantly at a constant rate of 0.5 m y^{-1} for 3 y (Fig. 4). We found that the transition between these two different stages of dune growth occurs for a mean slope of the order of 0.03, when dune crests and slip faces emerge and begin to spatially organize throughout the experimental plot. Steeper slopes highlight the increase in dune aspect ratio (Gadal et al., 2020; Phillips et al., 2019), which is the main control parameter for aerodynamic nonlinearities. Hence, we ascribe the two different stages to the linear and the nonlinear phases of the dune growth instability.

3.4 Experimental dispersion diagram

For each topographic survey, we performed a spectral decomposition of the elevation data to isolate the contribution of individual modes (wavelengths) to the overall topography. The variation of the amplitude of these surface waves is not homogeneous over time and displays a sudden change in rate at the end of 2014 (Fig. 5A) for a mean slope of the order of 0.03. We ascribe it to the transition from the linear to the nonlinear phases of the dune growth instability. During the linear phase, we obtain the experimental dispersion relation of the dune instability by plotting the growth rate of the different modes as a function of their wave number *k* (Fig. 5B). It provides eolian experimental evidence of the difference in growth rates of nascent dunes of various wavelengths when they are not large enough to generate flow recirculations. These results are consistent with the theoretical

prediction of the linear stability analysis with a clear maximum and a continuous trend from unstable (growing waves, $\sigma>0$) to stable regimes (decaying waves, $\sigma<0$). The most unstable mode corresponds to the wavelength of the emerging dune pattern in the field (≈15 m); the neutral mode ($\sigma=0$) is about 9 m (Richards, 1980).

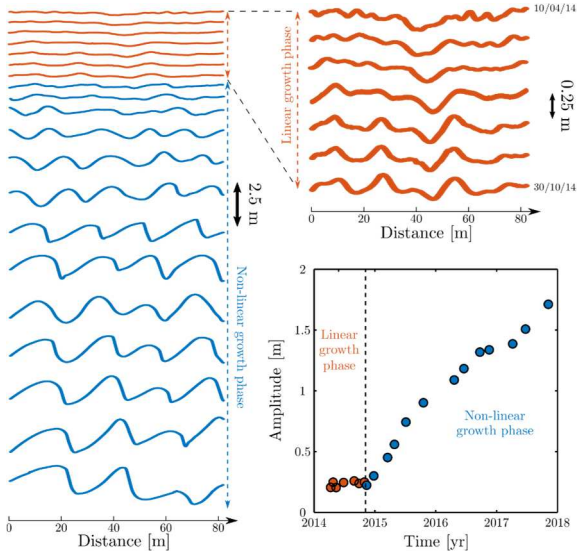

Figure 4. Dune growth in the flat sand bed experiment. Detrended elevation profiles along the same transect from 10 April 2014 to 7 November 2017 (left). Zoomed-in view of the elevation profiles from 10 April 2014 to 30 October 2014 shows the evolution of topography during the linear phase of dune growth (top right). The mean amplitude of bedforms with respect to time. Colors and dashed lines are used to separate the linear (orange) and the nonlinear (blue) phases of dune growth.

4 DISCUSSION

In order to meet the challenge of comparing and evaluating theoretical models of dune growth with observational data, the landscape-scale experiment conducted in an active dune field under the natural action of wind yields a unique set of quantitative relationships. By removing uncertainties about boundary and initial conditions, we verify that dunes can emerge from a flat sand bed and validate the theory behind this dune growth mechanism. We elucidate the origin of periodic bedforms, showing the wavelength selection as dunes increase in height. Meanwhile, we highlight the inherent benefits of combining field observations with theory to derive information about the sediment transport and flow properties from the morphodynamics of incipient dunes.

We provide an original dataset for an in-depth understanding of the linear phase of the dune instability, when the growth rates of the different modes evolve independently from each other (Lü et al. 2021). We find that this linear phase is at work from the earliest stage of dune growth, as soon as sand transport starts even when, at first glance, no regular structure seems to be in place. It takes time for the most unstable wavelength to prevail over all of the other modes that contribute to the sand bed topography. When periodic dunes are observed, the nonlinear phase has already taken over, aerodynamic nonlinearities have developed, and the different modes interact with each other to lead to pattern coarsening (Gao et al., 2015, Lü et al. 2022; Valance et al., 2010). We show here that the continuous transition from the linear to the nonlinear regimes is controlled by the dune aspect ratio for remarkably low values (≈0.03), consistent with laboratory measurements on sinusoidal beds (Charru et al. 2013). This transition coincides with the spatial organization of bedforms according to the alignment of mature dunes. For mean slope values of 0.07 (4°, typical of the flattest dune slopes), the transition is completed, and it is no longer possible to differentiate between the growth rates of the different modes. Nevertheless, the most unstable mode can still be observed to provide relevant length and timescales of the dune instability.

Our experiments bridge the gap between theoretical physics and geophysical surveys and can translate into concrete research avenues across scientific domains, in particular for river and marine dunes. Instability theory applies to many natural systems, especially to examine the relationships between flow and surface properties on subaqueous bedforms in rivers or oceans. For all these natural systems, we show here that, when the technological step in data acquisition is taken, field studies can

be carried out to test theoretical outputs against observations and to develop better forecasts of landscape morphogenesis.

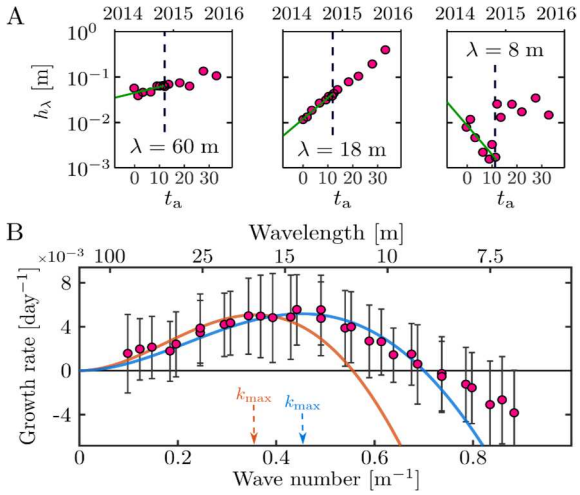

Figure 5. (A) Amplitudes of 60-, 18-, and 8-m wavelengths with respect to the dimensionless transport timescale t_a; t_a is set to zero on 10 April 2014. Two different regimes are observed before and after t_a=10.7, the 30 October 2014 (dashed lines). They are associated with the linear and nonlinear phases of dune growth. The growth rate of each wavelength (green lines) is determined by an exponential fit performed during the linear phase ($0 \leq t_a \leq 10.7$). (B) The experimental dispersion relation for the linear regime of the dune instability (i.e., the growth rate with respect to the wave number during the linear phase). Error bars show mean and standard deviation derived from 34 independent transects. Solid lines are dispersion relations using Eq. 1 and the best fit to the data $\{l_{sat}, A, B\}$={0.7, 1.96, 0.96} (blue) or the same parameters measured independently in the field $\{l_{sat}, A, B\}$={0.95, 3, 1.5} (orange). The most unstable wavelengths $\lambda_{max}=2\pi/k_{max}$ are equal to 14.6 and 18.5 m, respectively.

5 REFERENCES

Andreotti, B., Claudin, P., Pouliquen, O., 2010, Measurements of the aeolian sand transport saturation length. Geomorphology 123, 343–348.

Bagnold, R.A., 1941. The physics of wind blown sand and desert dunes. Methuen.

Charru, F., Andreotti, B., Claudin, P., 2013. Sand ripples and dunes. Annu. Rev. Fluid Mech., 45, 469–493.

Claudin, P., Wiggs, G. Andreotti, B., 2013. Field evidence for the upwind velocity shift at thecrest of low dunes. Boundary Layer Meteorol. 148, 195–206.

Elbelrhiti, H., Claudin, P., Andreotti B., 2005. Field evidence for surface-wave-induced instability of sand dunes. Nature 437, 720–723.

Gadal, C., Narteau, C, Courrech du Pont, S., Rozier, O., Claudin, P., 2019. Incipient bedforms in a bidirectional wind regime. J. Fluid Mech., 862, 490–516.

Gao, X., Narteau, C., Rozier, O., 2015, Development and steady states of transverse dunes: A numerical analysis of dune pattern coarsening and giant dunes. J. Geophys. Res., 120, 2200–2219.

Kennedy, J., 1963. The mechanics of dunes and antidunes in erodible bed channels. Journal of Fluid Mechanics, 16, 521–544.

Lü, P., Narteau, C., Dong, Z., Claudin, P., Rodriguez, S., An, Z., Fernandez-Cascales, L., Gadal, C., Courrech du Pont, S., 2021. Direct validation of the dune instability theory. Proceedings of the National Academy of Sciences, 18, e2024105118.

Lü, P., Narteau, C. , Dong, Z., Claudin, P., Rodriguez, S., An, Z., Gadal, C., Courrech du Pont, S., 2022. Coexistence of two dune growth mechanisms in a landscape-scale experiment. Geophysical Research Letters, 49, e2021GL097636.

Narteau, C., Zhang, D., Rozier, O., Claudin, P., 2009. Setting the length and time scales of a cellular automaton dune model from the analysis of superimposed bed forms. J. Geophys. Res. Earth Surf, 114, 1–18.

Phillips, J., et al., 2019. Low-angle eolian deposits formed by protodune migration, and insights into slipface development at white sands dune field, New Mexico. Aeolian Research, 36, 9–26.

Ping, L., Narteau, C., Dong, Z., Zhang, Z., Courrech du Pont, S., 2014, Emergence of oblique dunes in a landscape-scale experi-ment, Nat. Geosci., 7, 99–103.

Richards, K. J., 1980. The formation of ripples and dunes on an erodible bed. J. Fluid Mech., 99, 597–618.

Ungar, J., Haff, P., 1987. Steady state saltation in air. Sedimentology, 34, 289–299.

Valance, A., 2011. Nonlinear sand bedform dynamics in a viscous flow. Phys. Rev. E, 83, 036304.